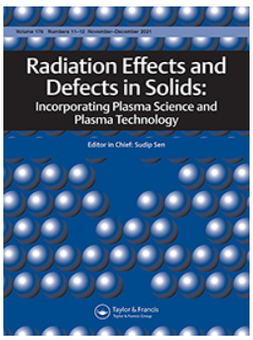

Taylor & Francis
Taylor & Francis Group

Radiation Effects and Defects in Solids
Incorporating Plasma Science and Plasma Technology

ISSN: (Print) (Online) Journal homepage: https://www.tandfonline.com/loi/grad20

Classification of thermoluminescence features of the natural halite with machine learning

Dilek Toktamis, Mehmet Bilal Er & Esme Isik

To cite this article: Dilek Toktamis, Mehmet Bilal Er & Esme Isik (2022): Classification of thermoluminescence features of the natural halite with machine learning, Radiation Effects and Defects in Solids, DOI: 10.1080/10420150.2022.2039927

To link to this article: https://doi.org/10.1080/10420150.2022.2039927

Published online: 21 Feb 2022.

RADIATION EFFECTS & DEFECTS IN SOLIDS
https://doi.org/10.1080/10420150.2022.2039927

Classification of thermoluminescence features of the natural halite with machine learning

Dilek Toktamis [a], Mehmet Bilal Er [b] and Esme Isik [c]

[a]Department of Physics Engineering, Faculty of Engineering, Gaziantep University, Gaziantep, Turkey;
[b]Department of Computer Engineering, Faculty of Engineering, Harran University, Şanlıurfa, Turkey;
[c]Department of Optician, Malatya Turgut Özal University, Malatya, Turkey

ABSTRACT

Radiation dosimeters are used to measure the absorbed radiation dose of any living organism during the time intervals. They include defective crystals that store radiation until they are stimulated. Thermoluminescence (TL) is a way to see the absorbed dose of the dosimeters. The irradiated crystal is heated up to 500°C to reveal the absorbed dose as a luminescence light. The TL dosimetric properties of natural halite (rock-salt) crystals extracted from Meke crater lake in Konya, Turkey, were investigated in this study. Support Vector Machine (SVM), Artificial Neural Network (ANN) and K-Nearest Neighbor (K-NN) were also examined utilizing machine learning for categorization of TL characteristics. According to the experimental output, the TL glow curve has two main peaks located at 100 and 270°C with good dosimetric properties. In the three classifiers, SVM has the biggest accuracy and precision. High training-low testing and results from normalized data give the best accuracy, precision, sensitivity and F-score.

ARTICLE HISTORY
Received 23 June 2021
Accepted 20 January 2022

KEYWORDS
Halite; thermoluminescence; machine learning

1. Introduction

The thermoluminescence (TL) phenomenon was widely used for dosimetric purposes and was first studied by Daniel et al [*1*]. TL is a defect-related phenomenon largely due to the presence of impurities and defects that can significantly affect the TL response and susceptibility materials, and various models have been proposed to explain the observation of glow curves (GLs) [*2*,*3*]. For obtaining information on the trapping states and defect distribution of insulators, the method is useful, convenient and effective. The energy levels in crystalline materials, on the other hand, are caused by structural defects or the presence of intrinsic and/or extrinsic atoms [*4*,*5*]. Depending on the processing conditions, electrons and holes formed as a result of irradiation of the material can be trapped at defect sites, and subsequent heating allows some of the stored energy to be released as photons [*6*,*7*].

Sodium chloride, or salt, is an ionic compound with the chemical formula NaCl, which represents the combination of sodium and chloride ions [*8*]. The basic structure is known

CONTACT Mehmet Bilal Er bilal.er@harran.edu.tr

as the halite or rock-salt crystal structure, and it can be present in a variety of other compounds. It can be interpreted as two interpenetrating face-centred cubic (fcc) lattices or as a face-centred cubic (fcc) lattice with a two-atom basis. It has wide bandgap energy that is about 8.5 eV [9]. NaCl is naturally crystallized from lakes, seawater mines as solid rock and also as saline groundwater. While impurities can affect the color spectrum of halite, defects within the crystal lattice are caused by the deep blue and violet colors, and bacteria from various algae cause the pink and peach colors of many dry lake halite specimens [10].

In general, the luminescence properties of natural halite have been investigated by some researchers [11–14] who observed two main peaks of halite and considered its use as a retrospective dosimeter [12,15–17]. The literature shows that natural halite is suitable and preferred for dosimetry studies [11,18,19]. In recent years, researchers used computational modeling tools to simulate and predict using data from their TL-OSL experimental work [20–25]. Artificial neural network [26–29] is the commonly used model for this purpose but deep learning [30] and machine learning [31] are also used. These proposed models have been presented to us with promising results.

In crystalline solids, there is a perfect order in the three-dimensional arrangement of the atoms, ions or molecules. Although a perfect crystal does not include any kind of defects, impurities or dislocations, there is no perfect crystal in the world. They include at least one of them. These defects and impurities in the solid crystals behave as a trap to store the ambient radiation until a kind of stimulation energy is applied. In thermoluminescence, the stimulation is done by heating the material to see the luminescence light.

In this study, the TL properties of natural Halite which are obtained from Meke crater lake, the town of Konya Karapinar, were investigated for the classification features by using machine learning. The proposed model consists of three classifiers which are as follows: Support Vector Machine (SVM), Artificial Neural Network (ANN) and K-Nearest Neighbor (K-NN), and were used for the classification process. Thus, it will be determined which method is more effective for classifying TL properties. A detailed description of the classifiers and methods are given in Section 2. Their detailed results are given in Section 3.

2. Materials and methods

In this part of the study, the halite samples collected from the dry lake layer were divided into four main groups to obtain TL characteristics such as dose–response, fading, reproducibility and heating rates. For all parts of the experiment, samples of 20 mg were weighed and irradiated with a β-source at room temperature, and the irradiated samples were read by the Harshaw TLD System 3500 Manual TLD Reader at 1°C/s. The dose rate of the point beta source (^{90}Sr–^{90}Y) is 0.040 Gy/s and its activity was about 3.7 GBq (100 mCi). The β-source was installed in a 9010 optical dating system which is interfaced to a PC using a serial RS-232 port to control irradiation time. It is calibrated by the manufacturer on 10 March 1994. A standard clear glass filter was always installed in the TLD reader between the planchet and photomultiplier tube to eliminate unwanted infrared light that is emitted from the heater. For the dose–response experiment, samples were irradiated from 2.4 Gy to 108 Gy and the irradiated samples were read at 1°C/s by the TLD reader. In the reproducibility part of the experiment, all samples were irradiated with 36 Gy and read out at 1°C/s and this step was repeated five times. For the fading studies, all samples were irradiated with 36 Gy and stored in the darkroom for various periods of time before being read

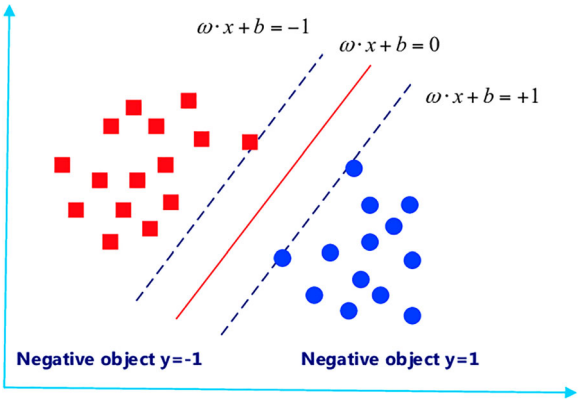

Figure 1. Support vector machine.

out at 1°C/s. Halite samples were likewise irradiated with 36 Gy and then read out for different heating rates using the TLD reader in the heating rate experiment. The proposed methodology for the classification of the glow curve data of halite obtained as a result of all these experiments and its main components is discussed in detail. The proposed method consists of three main stages. In the first step, a dataset was created by labeling the items manually with dose–response, heating rate, reproducibility and fading class labels according to the temperature and TL intensity values obtained as a result of the experiment. In the second step, the data were pre-processed and normalized. In the last step, Support Vector Machine (SVM), K-Nearest Neighbor (K-NN) and Artificial Neural Network (ANN) machine learning algorithms were trained using temperature and TL intensity features.

2.1. Support vector machine

Support Vector Machine (SVM) is one of the most robust machine learning techniques that can be decomposed by linear and non-linear lines derived from Vapnik's statistical learning theory [32]. This technique can be used for both classification and regression analysis and is a supervised learning method for classifying small data [33]. In SVM, the input data are first transferred to a high-dimensional space where two groups can be separated by a hyperplane that maximizes the margin between them [34]. It is ideal that the wider the space between the two classes in SVM, the classification will be more successful. SVM that separates the two classes in the optimal hyperplane is given in Figure 1.

The optimal hyperplane $f(x) = 0$ between datasets is composed by SVM by solving a constrained quadratic optimization problem based on inherent risk minimization [35].

x_i, $i = 1,,\ldots,n$ input vector $y_i - 1$, 1 belongs to one of two classes, the hyperplane is defined as:

$$w_0.x + b_0 = 0 \tag{1}$$

Here w, x and b indicate the weight vector, input vector and bias, respectively. For a given w and b, the data can be linearly divided in the following cases:

$$w.x_i + b \geq 1 \text{ if } y_i = 1 \tag{2}$$

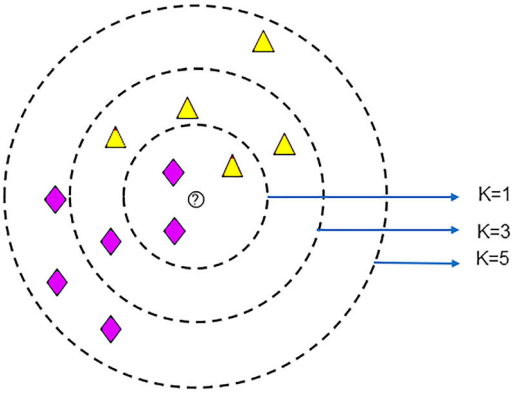

Figure 2. K-NN diagram.

$$w.x_i + b \leq 1 \text{ if } y_i = -1 \tag{3}$$

The kernel method is used to solve a non-linear problem with a linear classifier. The input data are transformed into a higher dimensional feature space with the function Φ. K kernel function:

$$k(x, x') = ((x), (x' \tag{4}$$

- Polynomial

$$k(x_i, x_j) = (x_i.x_j + 1)^d \tag{5}$$

- Radial Basis Function

$$(x, y) = e^{-\gamma||(x-x_i||^2} \tag{6}$$

2.2. K-nearest neighbor

K-NN algorithms hypothesize to categorize a data subset that is defined as similarity measure to query its K-nearest neighbors from a large-scale data set. It is used as a basic component in a wide range of applications such as dimension reduction, pattern recognition and image acquisition [36,37]. K-NN is a learning algorithm based on the principle that samples in a dataset will often be found near other samples with similar characteristics [38]. With this algorithm, there are k training points nearest to this point data to classify a new point data. The classification occurs by the majority vote of the neighbors. A component to be classified is distributed to the nearest class among the nearest neighbors measured by a distance function [39]. The formulation of the K-NN algorithm is shown in Equation (7).

$$x(x, y) = \sqrt{\sum_{j=1} w_j (x_j - z_j)^2} \tag{7}$$

In Equation (7); w_j is the weight associated with the j dimension. The weight is selected for each dimension and the square distance function is specified. K-NN diagram is given in Figure 2.

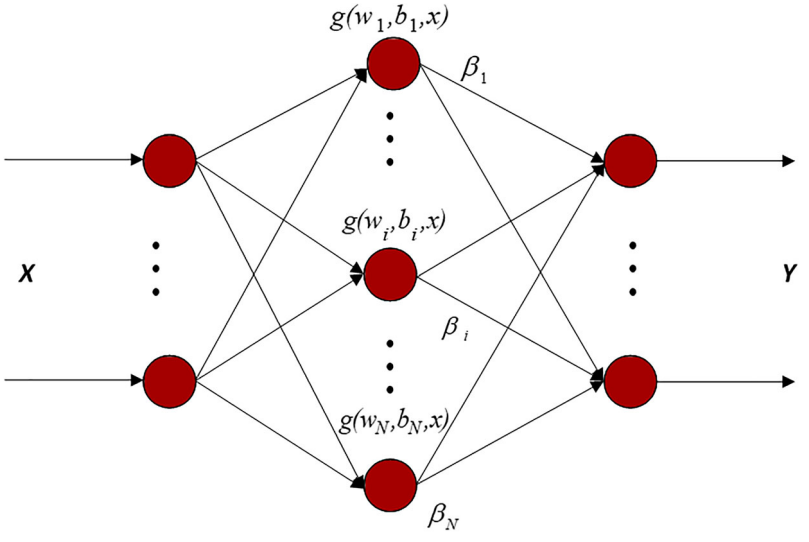

Figure 3. Artificial neural network.

2.3. Artificial neural network

ANN is inspired by the intelligent data processing capability of the human brain. ANN is motivated by imitating the interaction of neurons in the brain with each other [40]. The ANN model, which is a mathematical model consisting of neurons and associated neuron connections, is shown in Figure 3. The connections formed between neurons used in network formation are associated with numerical values called weights. Each weight has a certain value that is transferred in the network and multiplied by the data samples [41,42]. ANNs can be trained to recognize non-linear relationships between input and output data without having knowledge about the problem. After training, the runtime of ANN is extremely fast because it contains only a few simple, interconnected processing units. ANNs have features such as model recognition, generalization and interpolation. Therefore, when an unknown input is applied to the trained network, it can produce a suitable output. They require only simulated training data rather than deterministic error and system models [43].

3. Experimental applications

3.1. Experimental results

In this study, the TL dosimetric properties of the natural halite (rock-salt) crystals were investigated by using machine learning for the classification features. The halite material exhibits good TL dosimetric properties, such as a simple TL glow curve with two distinct peaks, as seen in Figure 4. Although the first peak is unsuitable for dosimetric applications due to its easy fading at low temperatures, the second peak is in the appropriate temperature range. The appropriate temperature range means no loss is observed in the radiation dose stored in the defect responsible for this peak and all stored radiation dose in this defect is easily measured by applying suitable thermal energy.

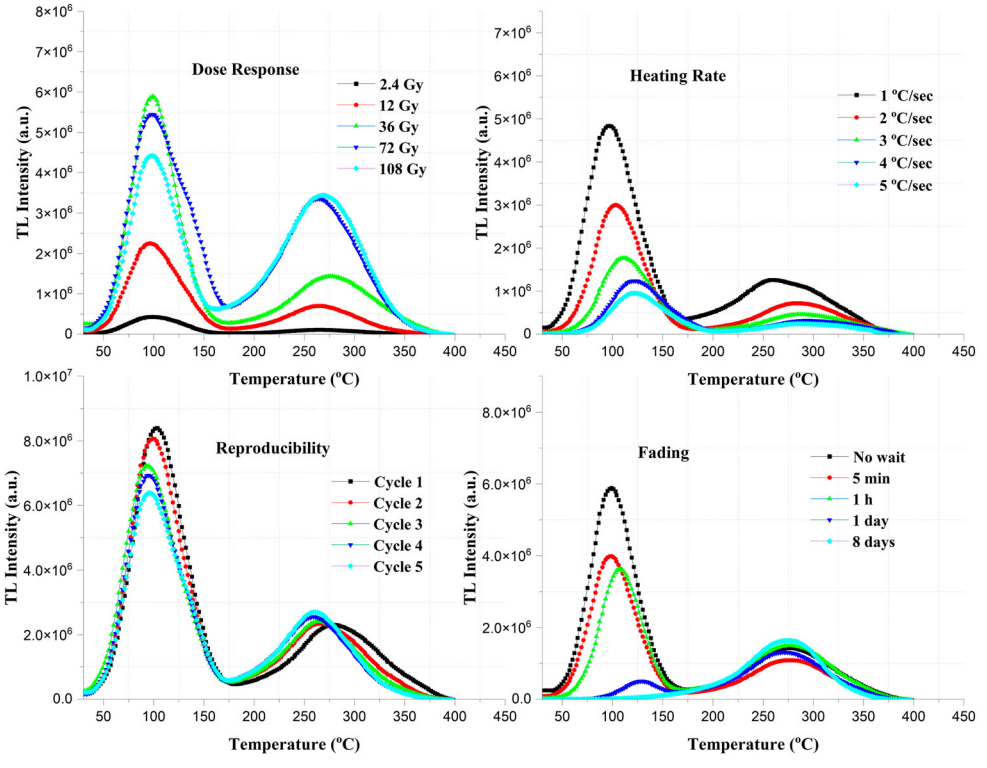

Figure 4. The glow curve variations of Halite samples with respect to the dose response, heating rate, reproducibility and fading.

SVM, ANN and K-NN were used for the classification process of the glow curve data of halite samples. Before the classifiers were trained, the data were normalized by pre-processing. SVMs are trained using Polynomial and Radial Basis Function kernels. For K-NN, the number of K was chosen as 3. The data were divided into two different ways to determine the effect of the data size allocated for training and testing on the classifier. First, 70% of the data were used for training, 30% for testing; second, 80% of the data were used for training and 20% for testing. Different machine learning algorithms were trained in the study to analyze the dataset including TL glow curve data. After that, the results of the experiments were analyzed using the classification metrics. To measure the performance of machine learning algorithms, there are common classification metrics available. The quality of the model was evaluated using classification metrics. The performance of the model was measured using classification metrics such as accuracy, precision, sensitivity and F-score. The evaluation criteria in classification problems are performed by using a matrix, called the confusion matrix, with the correct and incorrectly classified sample numbers for each class. The descriptions of FP, FN, TP and TN can be defined as follows:

- False positives (FP): samples of negative class, predicted positively.
- False negatives (FN): negatively predicted samples with a positive true class.
- True positives (TP): correctly predicted examples of the positive class.
- True negatives (TN): examples that are correctly predicted as belonging to the negative class.

Table 1. Classification results from non-normalized data.

Model	Dividing data at different rates for training and testing	Accuracy %	Precision %	Sensitivity %	*F*-score %
SVM (Polinom)	30%–70%	95.22	94.24	95.64	94.65
SVM (Polinom)	20%–80%	**96.10**	95.62	95.87	95.04
SVM (RBF)	30%–70%	94.23	94.70	94.51	95.41
SVM (RBF)	20%–80%	95.14	95.71	95.05	95.64
K-NN	30%–70%	92.45	94.00	95.86	94.10
K-NN	20%–80%	93.36	94.88	94.85	95.99
ANN	30%–70%	95.24	94.83	94.37	94.40
ANN	20%–80%	95.45	95.35	94.94	95.07

$$\text{Accuracy} = \frac{|TN| + |TP|}{|FN| + |FP| + |TN| + |TP|} \tag{8}$$

Precision measurement evaluates the efficiency of the classifier for each class in binary problems. Sensitivity, known as the true positive rate, is the ratio of predicted data from the positive class to the true positive data. The formulation of precision is given in Equation 9.

$$\text{Precision} = \frac{|TP|}{|FN| + |TP|} \tag{9}$$

Sensitivity is a measure of the probability that a positive prediction is correct. Sensitivity measurement is given in Equation 10.

$$\text{Sensitivity} = \frac{|TP|}{|TP| + |FN|} \tag{(10)}$$

The *F*-score is a harmonious mean of positive predictive ratio and sensitivity measures. The reason why it is a harmonic mean instead of a simple mean is that we should not ignore the extreme cases. Positive predictive ratio and sensitivity measures alone are not sufficient to draw a meaningful comparison result. Since evaluating both criteria together gives more accurate results, F-score is defined. The *F*-score is calculated as in Equation 11.

$$F\text{ - score} = \frac{2*|TP|}{2*|TP| + |FP| + |FN|} \tag{11}$$

In the first experiment, the classifiers were trained without normalizing the data, and in the second experiment, the classifiers were trained by normalizing the data. The classification results obtained from the data that cannot be normalized are given in Table 1. The highest accuracy is acquired as 96.10% when SVM is used with the polynomial kernel, and the highest accuracy value is obtained as 95.14% when the SVM is used with the RBF kernel. In addition, the highest accuracy was obtained 93.36% with K-NN and the highest accuracy is acquired as 95.45% with ANN. In terms of accuracy, the best classification performance was obtained with the SVM classifier. The confusion matrix for the best classification result obtained with non-normalized data is given in Figure 5.

The classification results obtained after the data are normalized and are given in Table 2. The highest accuracy value is acquired at 99.20% when SVM is used with the polynomial kernel, and the highest accuracy is obtained as 98.11% when it is used with the RBF

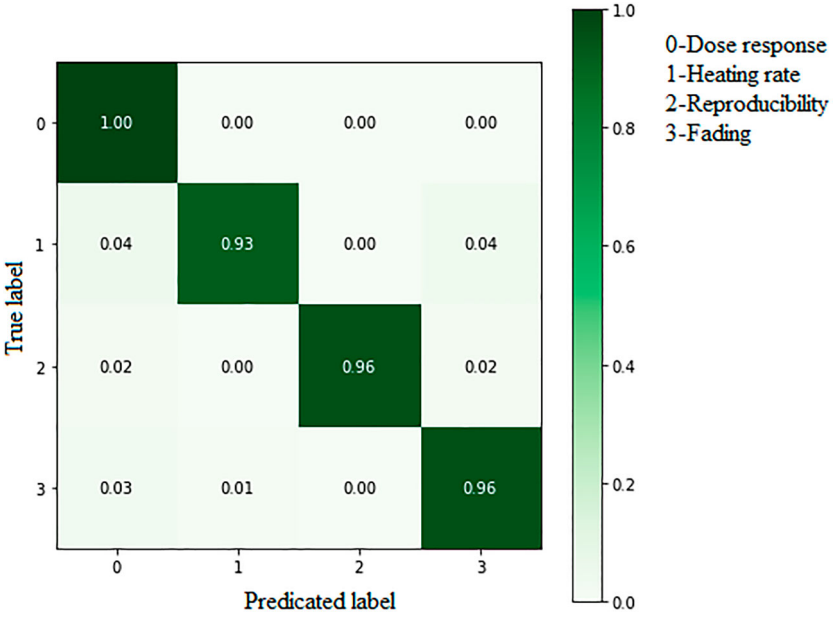

Figure 5. Confusion matrix for the best classification result with unnormalized data.

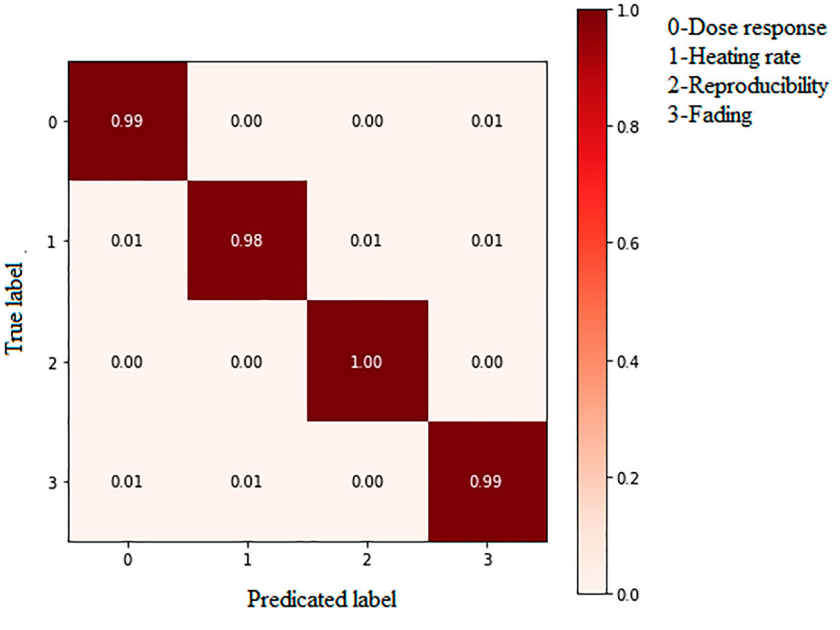

Figure 6. Confusion matrix for the best classification result with normalized data.

kernel. In addition, the highest accuracy was 97.23% with K-NN and the highest accuracy was 95.14% with ANN. The best classification performance with respect to the accuracy was again obtained with the SVM classifier. The confusion matrix for the best classification result obtained with normalized data is given in Figure 6.

Table 2. Classification results obtained from normalized data.

Model	Dividing data at different rates for training and testing	Accuracy %	Precision %	Sensitivity %	*F*-score %
SVM (Polinom)	30%–70%	97.56	97.96	98.49	97.35
SVM (Polinom)	20%–80%	**99.20**	99.08	98.88	98.88
SVM (RBF)	30%–70%	97.24	97.12	97.52	98.45
SVM (RBF)	20%–80%	98.11	98.29	98.34	98.54
K-NN	30%–70%	96.46	97.33	97.51	97.87
K-NN	20%–80%	97.23	98.03	97.74	99.12
ANN	30%–70%	98.23	97.62	97.00	97.04
ANN	20%–80%	99.14	98.30	98.93	99.01

All experiments must be done manually in a laboratory setting to interpret TL characteristics by looking at the TL glow curve. At the same time, experimental studies in the laboratory environment are dangerous and take a long time. In addition, the materials used in the experiments are quite expensive. To accelerate and facilitate the analysis of TL dosimetric features, machine learning software, which is a sub-branch of artificial intelligence, was used in this study. The proposed classification models of TL glow curves derived from four distinct experiments were shown to have high accuracy rates in this study. These results showed that the thermoluminescence glow curves of dosimetric materials can be used for the classification method. Therefore, we can obtain information about dose–response and fading times of TL glow curves. In this way, it will be possible to have information about the fading time of the TL glow curves, heating rates and dose rates without experimental knowledge. According to the glow curve data, the researchers simulated and predicted the TL intensity [*22*,*44*], fading time [*20*,*23*,*45*], the date or source of exposure [*46*] and dose rate [*23*] by using machine learning. And, one can obtain the kinetic parameters such as activation energy and frequency factor to determine the defect center of TL materials using some other methods according to the glow curve data [*47*,*48*]. In this study, TL characteristics such as dose–response, fading time, reproducibility and heating rate are classified, and in this way, the TL glow curve data determine which TL characteristic they belong to, and thus the amount of exposed dose and the fading time will be determined.

4. Conclusion and future work

The TL dosimetric properties of natural halite (rock-salt) crystals recovered from Meke crater lake in Konya, Turkey, were investigated in this work. Machine learning was used to study the classification of their features. The halite material has good TL dosimetric properties, such as a simple TL glow curve with two distinguishable peaks, when the results are examined according to their dosimetric features. Machine learning with three classifiers was used to analyze the TL outcomes for classification characteristics. SVM, ANN and K-NN were chosen for the classification process. Results were tabulated and compared as normalized and non-normalized data. When divided, data are chosen as 80% training and 20% testing, and the better accuracy, precision, sensitivity and F-score are obtained. Results from normalized data give better accuracy, precision, sensitivity and F-score than unnormalized data. In the chosen classifiers, the SVM has the biggest accuracy and precision than others, and both results obtained from normalized and non-normalized data.

In short, the halite crystal extracted from Meke crater lake in Konya city of Turkey shows good dosimetric properties, and SVM which is used as a classifier for machine learning has the biggest accuracy and precision. High training-low testing gives the best accuracy, precision, sensitivity and F-score. In future work, we can try to learn about the defect centers involved in the TL glow curves by regression method.

Disclosure statement

No potential conflict of interest was reported by the author(s).

Notes on contributors

Dilek Toktamis was born in Gaziantep, Turkey. He received the B.S. degrees in physics teacher from the University of Diyarbakır, Turkey, in 1997. M.S. degrees in physics engineering from the University of Gaziantep, Turkey, in 2002 and the Ph.D. degree in also physics engineering from Gaziantep University, in 2017. Her research interests include solid state physics, thermoluminescence.

Mehmet Bilal Er received the B.S. degree in computer engineering from Eastern Mediterranean University, Cyprus, in 2010, the M.Sc. degree in computer engineering from Cankaya University, Turkey, in 2013, and the Ph.D. degree in computer engineering from Maltepe University, Turkey, in 2019. He is currently an Assistant Professor with the School of Computer Engineering, Harran University.

Esme Isik was born in Gaziantep, Turkey. He received the B.S. and M.S. degrees in physics engineering from the University of Gaziantep, Turkey, in 2013 and the Ph.D. degree in also physics engineering from Gaziantep University, in 2019. From 2012 to 2019, she was a Research Assistant with the Gümüshane University in Engineering Physics. Since 2019, she has been an Assistant Professor with the Mechanical Malatya Turgut Ozal University, Malatya. Her research interests include solid state physics, thermoluminescence, artificial neural network.

ORCID

Dilek Toktamis http://orcid.org/0000-0002-0333-1740
Mehmet Bilal Er http://orcid.org/0000-0002-2074-1776
Esme Isik http://orcid.org/0000-0002-6179-5746

References

(1) Daniels, F.; Boyd, C.A.; Saunders, D.F. *Thermoluminescence as a research tool. Science* **1953**, *117*, 343.
(2) McKeever, S.W. *Thermoluminescence of Solids*; Cambridge University Press: Cambridge, 1985.
(3) Chen, R.K. *Analysis of Thermally Stimulated Processes*. 1987.
(4) Bos, A.J.J. High Sensitivity Thermoluminescence Dosimetry. *Nucl. Instrum. Methods Phys. Res. Sect. B Beam Interact with Mater. Atoms.* **2001,** *184*, 3–28.
(5) Kortov, V. Materials for Thermoluminescent Dosimetry: Current Status and Future Trends. *Radiat. Meas.* **2007,** *42*, 576–581.
(6) Bhatt, B.C. Thermoluminescence, Optically Stimulated Luminescence and Radiophotoluminescence Dosimetry: An Overall Perspective. *Radiat. Prot. Environ.* **2011,** *34* (1), 6.
(7) Rivera, T. Thermoluminescence in Medical Dosimetry. *Appl. Radiat. Isot.* **2012,** *71*, 30–34.
(8) Kumar, D.; Ahmad, N.; Kumar, V.; Jha, V.K.; Kulshrestha, S.; Saini, R.et al, Various Polarization Mechanisms Involved in Ionic Crystals. 3Rd Int Conf Condens Matter. *Appl. Phys.* 2020, *2220*, 040036.
(9) Poole, R.T.; Liesegang, J.; Leckey, R.C.G.; Jenkin, J.G. Electronic Band Structure of the Alkali Halides. II. Critical Survey of Theoretical Calculations. *Phys. Rev. B* **1975,** *11*, 5190–5196.

(10) Ftncrn, L.W. A Revised Method of Operation of the Single-Crystal Diamond Cell and Refinement of the Stiucture of NaCl at 32 kbar X-roy. *Am. Mineral.* **1978**, *63*, 337–342.
(11) Rodriguez-Lazcano, Y.; Correcher, V.; Garcia-Guinea, J. Luminescence Emission of Natural NaCl. *Radiat. Phys. Chem.* **2012,** *81*, 126–130.
(12) Majgier, R.; Biernacka, M.; Palczewski, P.; Mandowski, A.; Polymeris, G.S. Investigation on Thermally Assisted Optically Stimulated Luminescence (TA – OSL) Signal in Various Sodium Chloride Samples. *Appl. Radiat. Isot.* **2019,** *143*, 98–106.
(13) Majgier, R.; Biernacka, M.; Mandowski, A. Properties of the Model for Radiation Induced Optically Stimulated Luminescence (OSL) in Sodium and Potassium Chlorides. *Radiat. Meas.* **2019,** *127*, 106142.
(14) Shahein, A.Y.; Hafez, H.S.; Abdou, N.Y. Retrospective Dosimetry Using Egyptian Halite (NaCl). *J. Radiat. Res. Appl. Sci.* **2019,** *12*, 311–318.
(15) Bailey, R.M.; Adamiec, G.; Rhodes, E.J. OSL Properties of NaCl Relative to Dating and Dosimetry. *Radiat. Meas.* **2000,** *32*, 717–723.
(16) Mesterházy, D.; Osvay, M.; Kovács, A.; Kelemen, A. Accidental and Retrospective Dosimetry Using TL Method. *Radiat. Phys. Chem.* **2012,** *81*, 1525–1527.
(17) Biernacka, M.; Majgier, R.; Maternicki, K.; Liang, M.; Mandowski, A. Peculiarities of Optically Stimulated Luminescence in Halite. *Radiat. Meas.* **2016,** *90*, 247–251.
(18) Ahmad, K.; Kakakhel, M.B.; Hayat, S.; Wazir-ud-Din, M.; Mahmood, M.M.; Ur Rehman, S.et al, Thermoluminescence Study of Pellets Prepared Using NaCl from Khewra Salt Mines in Pakistan. *Radiat. Environ. Biophys.* **2021**, *3*, 2.
(19) Khamis, F.M.; Arafah, D.E. Improved Thermoluminescence Properties of Natural NaCl Salt Extracted From Mediterranean Sea Water Relevant to Radiation Dosimetry. *Eur. J. Appl. Phys.* **2020,** *2*, 1–6.
(20) Isik, I.; Isik, E.; Toktamis, H. Dose and Fading Time Estimation of Glass Ceramic by Using Artificial Neural Network Method. *DÜMF Mühendislik. Derg.* **2020,** *12*, 47–52.
(21) Isik, E.; Toktamis, H.; Isik, I. Analysis of Thermoluminescence Characteristics of a Lithium Disilicate Glass Ceramic Using a Nonlinear Autoregressive with Exogenous Input Model. *Luminescence* **2020**, *35*, 1–8.
(22) Kucuk, N.; Kucuk, I. Computational Modeling of Thermoluminescence Glow Curves of Zinc Borate Crystals. *J. Inequal. Appl.* **2013**, *2013*, 1–7.
(23) Theinert, R.; Kröninger, K.; Lütfring, A.; Mender, S.; Mentzel, F.; Walbersloh, J. Fading Time and Irradiation Dose Estimation from Thermoluminescent Dosemeters Using Glow Curve Deconvolution. *Radiat. Meas.* **2018,** *108*, 20–25.
(24) Theinert, R.; Kröninger, K.; Lütfring, A.; Walbersloh, J. Computational Analysis of Thermoluminescence Glow Curves from Thin Layer Dosemeters. *Radiat. Meas.* **2017,** *106*, 252–256.
(25) Lee, S.Y.; Kim, B.H.; Lee, K.J. An Application of Artificial Neural Intelligence for Personal Dose Assessment Using a Multi-Area OSL Dosimetry System. *Radiat. Meas.* **2001,** *33*, 293–304.
(26) Rafiq, M.Y.; Bugmann, G.; Easterbrook, D.J. Neural Network Design for Engineering Applications. *Comput. Struct.* **2001,** *79*, 1541–1552.
(27) Aggarwal, C.C. Neural Networks and Deep Learning. **2018**.
(28) Bayraktar, Y.; Özyılmaz, A.; Toprak, M.; Işık, E.; Büyükakın, F.; Olgun, M.F. Role of the Health System in Combating Covid-19: Cross-Section Analysis and Artificial Neural Network Simulation for 124 Country Cases. *Soc. Work. Public. Health.* **2020,** *36*, 1–16.
(29) Isik, E.; Isik, I.; Toktamis, H. Analysis and Estimation of Fading Time from Thermoluminescence Glow Curve by Using Artificial Neural Network. *Radiat. Eff. Defects Solids* **2021,** *176*, 765.
(30) Arnold, L.; Rebecchi, S.; Chevallier, S.; Paugam-Moisy, H. An introduction to deep learning. ESANN 2011. 19th Eur Symp Artif Neural Networks 2011, 477–88.
(31) Kubat, M. An Introduction to Machine Learning. **2017**.
(32) Support Vector Machines. Boser, Guyon, Vapnik. SpringerReference 1992, Springer-Verlag, n.d.
(33) Widodo, A.; Yang, B.-S. Support Vector Machine in Machine Condition Monitoring and Fault Diagnosis. *Mech. Syst. Signal. Process.* **2007,** *21*, 2560–2574.
(34) Kabir E, S.; Zhang, Y. Epileptic Seizure Detection from EEG Signals Using Logistic Model Trees. *Brain. Inform.* **2016,** *3*, 93–100.

(35) Schölkopf, B.; Smola AJ. Smola, A. *Learning with Kernels – Support Vector Machines, Regularization, Optimization and Beyond*. MIT Press, Cambridge, 2001.
(36) Zhang, Y.; Ji, X.; Zhang, S. An Approach to EEG-Based Emotion Recognition Using Combined Feature Extraction Method. *Neurosci. Lett.* **2016,** *633*, 152–157.
(37) Jégou, H.; Douze, M.; Schmid, C. Product Quantization for Nearest Neighbor Search. *IEEE Trans. Pattern Anal. Mach. Intell.* **2011,** *33*, 117–128.
(38) Cover, T.; Hart, P. Nearest Neighbor Pattern Classification. *IEEE Trans. Inf. Theory* **1967,** *13*, 21–27.
(39) Li, C.; Zhang, S.; Zhang, H.; Pang, L.; Lam, K.; Hui, C.et al, Using the K-Nearest Neighbor Algorithm for the Classification of Lymph Node Metastasis in Gastric Cancer. *Comput. Math. Methods. Med.* **2012**, *2012*, 1–11.
(40) Chien, S.I.-J.; Ding, Y.; Wei, C. Dynamic Bus Arrival Time Prediction with Artificial Neural Networks. *J. Transp. Eng.* **2002,** *128*, 429–438.
(41) Pappu, S.M.J.; Gummadi, S.N. Artificial Neural Network and Regression Coupled Genetic Algorithm to Optimize Parameters for Enhanced Xylitol Production by Debaryomyces Nepalensis in Bioreactor. *Biochem. Eng. J.* **2017,** *120*, 136–145.
(42) Yang, Q.; Le Blond, S.; Aggarwal, R.; Wang, Y.; Li, J. New ANN Method for Multi-Terminal HVDC Protection Relaying. *Electr. Power Syst. Res.* **2017,** *148*, 192–201.
(43) Niebur, D.; Germond, A.J. Power Flow Classification for Static Security Assessment. Proc First Int Forum Appl Neural Networks to Power Syst, n.d.
(44) Pathan, M.S.; Pradhan, S.M.; Palani Selvam, T. Machine Learning Algorithms for Identification of Abnormal Glow Curves and Associated Abnormality in CaSO4:Dy-Based Personnel Monitoring Dosimeters. *Radiat. Prot. Dosimetry* **2020,** *190*, 342–351.
(45) Kröninger, K.; Mentzel, F.; Theinert, R.; Walbersloh, J. A Machine Learning Approach to Glow Curve Analysis. *Radiat. Meas.* **2019,** *125*, 34–39.
(46) Mentzel, F.; Derugin, E.; Jansen, H.; Kröninger, K.; Nackenhorst JW and JW, O. No More Glowing in the Dark: How Deep Learning Improves Exposure Date Estimation in Thermoluminescence Dosimetry. *J. Radiol. Prot. Accept.* **2020**, *41*, 0–6.
(47) Topaksu, M.; Yazici, A.N. The Thermoluminescence Properties of Natural CaF2 After β Irradiation. *Nucl. Instr. Methods Phys. Res. Sect. B* **2007**, *264*, 293–301.
(48) Annalakshmi, O.; Jose, M.T.; Madhusoodanan, U.; Venkatraman, B.; Amarendra, G. Kinetic Parameters of Lithium Tetraborate Based TL Materials. *J. Lumin.* **2013,** *141*, 60–66.